Positive pion-nucleus elastic scattering at 30 and 50 MeV

B. M. Preedom, S. H. Dam,* C. W. Darden III, R. D. Edge, D. J. Malbrough,† and T. Marks*
University of South Carolina, Columbia, South Carolina 29208

R. L. Burman, M. Hamm, M. A. Moinester,‡ R. P. Redwine,§ and M. A. Yates
Los Alamos Scientific Laboratory, Los Alamos, New Mexico 87545

F. E. Bertrand, T. P. Cleary, E. E. Gross, N. W. Hill, and C. A. Ludemann
Oak Ridge National Laboratory, Oak Ridge, Tennessee 37830

M. Blecher, K. Gotow, D. Jenkins, and F. Milder‖
Virginia Polytechnic Institute and State University, Blacksburg, Virginia 24061
(Received 18 August 1980)

We present measured angular distributions for π^+-elastic scattering at 30 and 50 MeV from selected targets with $A = 12$ to 208. These angular distributions were analyzed using a phenomenological optical potential of first-order form. The mass dependence of the potential strength parameters displays the isospin dependence expected from the free πN interaction.

[NUCLEAR REACTIONS Elastic scattering of 30 and 50 MeV π^+ from ^{12}C, ^{16}O, ^{40}Ca, ^{90}Zr, ^{208}Pb. Angular distributions: $25° < \theta_{LAB} < 160°$. Optical model analysis of cross-section data.]

I. INTRODUCTION

Low energy pion elastic scattering has proven to be a rich area of study for information about the pion-nucleus interaction. Unlike the energy region near the πN (3,3) resonance, at low energies ($\lesssim 80$ MeV) the pion penetrates the nucleus beyond the surface and thus the interaction is sensitive to the interior nuclear density. First-order optical potentials derived from the free πN scattering amplitudes in a multiple-scattering formalism have been shown to be totally inadequate to describe low-energy pion-nucleus elastic scattering data.[1-3] Second order corrections which allow for annihilation of the incident pions and correlations between the nucleons have been shown to be necessary for even a qualitative description of the data.[1-10] Although there is currently disagreement as to how these second-order effects should be included, there is no disagreement about their importance.

Several measurements of low-energy pion-nucleus ($A > 4$) elastic scattering have already been published[11-15] and have been summarized in reviews.[16,17] The measurements presented here and in a recent communication[18] represent a substantial increase in the mass range studied and will make a systematic mass and energy dependent analysis possible. We present angular distributions for the elastic scattering of π^+ from ^{12}C, ^{16}O, ^{40}Ca, ^{90}Zr, and ^{208}Pb at energies of 30 and 50 MeV. We have previously published π^+ elastic scattering data from ^{12}C and ^{16}O at 50 MeV.[11,13] These earlier data are summarized here for completeness. The particular targets were chosen because they are all "core" nuclei in their respective mass regions.

We have analyzed the present data using a phenomenological optical potential of first order form whose strength parameters have been adjusted to fit the data. The parameters thus obtained are examined for any systematic trends with mass and/or energy.

II. EXPERIMENTAL PROCEDURE

The experimental procedure for our measurements has been discussed in detail in a previous publication.[11] We review here the salient features of our measurements.

We used the pion beam from the Low Energy Pion Channel[19] (LEP) at the Clinton P. Anderson Meson Physics Facility at the Los Alamos Scientific Laboratory (LAMPF). The beam momentum resolution was chosen to be $\Delta p/p = 2.0\%$ at 30 MeV and 1.0% at 50 MeV. The beam spot size [full width at half maximum (FWHM)] on target was 1.4 cm (vertical) by 2 cm (horizontal) at 30 MeV and 0.8 cm × 2 cm at 50 MeV.

The beam profile was measured by an in-beam current-sensitive wire chamber[20] with wire spacings of 1 mm. During data runs at 30 MeV, the

beam intensity was monitored by a "decay-muon" telescope[21] consisting of two detectors in coincidence, set at an angle with respect to the beam of approximately half of the maximum laboratory angle for the muon from the $\pi \rightarrow \mu\nu$ decay. At 50 MeV, the beam intensity was monitored by using two plastic scintillators which detected coincident protons from $(\pi^+, 2p)$ reactions in the target. Both the decay-muon telescope and the $(\pi^+, 2p)$ monitor were calibrated against an in-beam telescope consisting of two plastic scintillator counters which were each 1.27 cm thick for the 30 MeV beam and 2.54 cm thick for the 50 MeV beam. By recording the pulse height in one counter versus that in the other counter, it was possible to separate the electrons and muons in the beam from the pions. A representative spectrum showing this separation for the 50 MeV beam is displayed in Fig. 1. For these calibrations, the momentum spread of the channel was decreased to provide an average counting rate of $\lesssim 5 \times 10^5$ counts/sec in the in-beam detectors. Slits in the front half of the channel which define the phase space transmitted through the channel were unchanged between the full intensity and low intensity runs.

Consistency checks of the calibration were made during the different data runs by a comparison of cross sections obtained in detectors having the same scattering angles and by a comparison of the muon telescope counting rate with that of a detector monitoring the primary proton current. These checks indicated a consistency of better than 3% for the relative normalizations.

The differential cross sections were measured in the vertical plane using a ten-counter array of plastic scintillator telescopes[22] consisting of a solid-angle defining, thin ΔE counter and a thick stopping E counter. Each detector subtended a solid angle of ~4 msr. In order to reduce the background due to muons from the decaying pion beam for detectors at angles of 45° or less, we required the identification of the 4 MeV muon pulse[23] resulting from the decay of the stopped π^+. The efficiency of these detectors was determined by placing them in the incident pion beam and measuring the number of pions detected with and without the 4 MeV muon detection requirement. Also, these detectors were compared with simple detectors at large scattering angles where the muon background is insignificant. These mea-

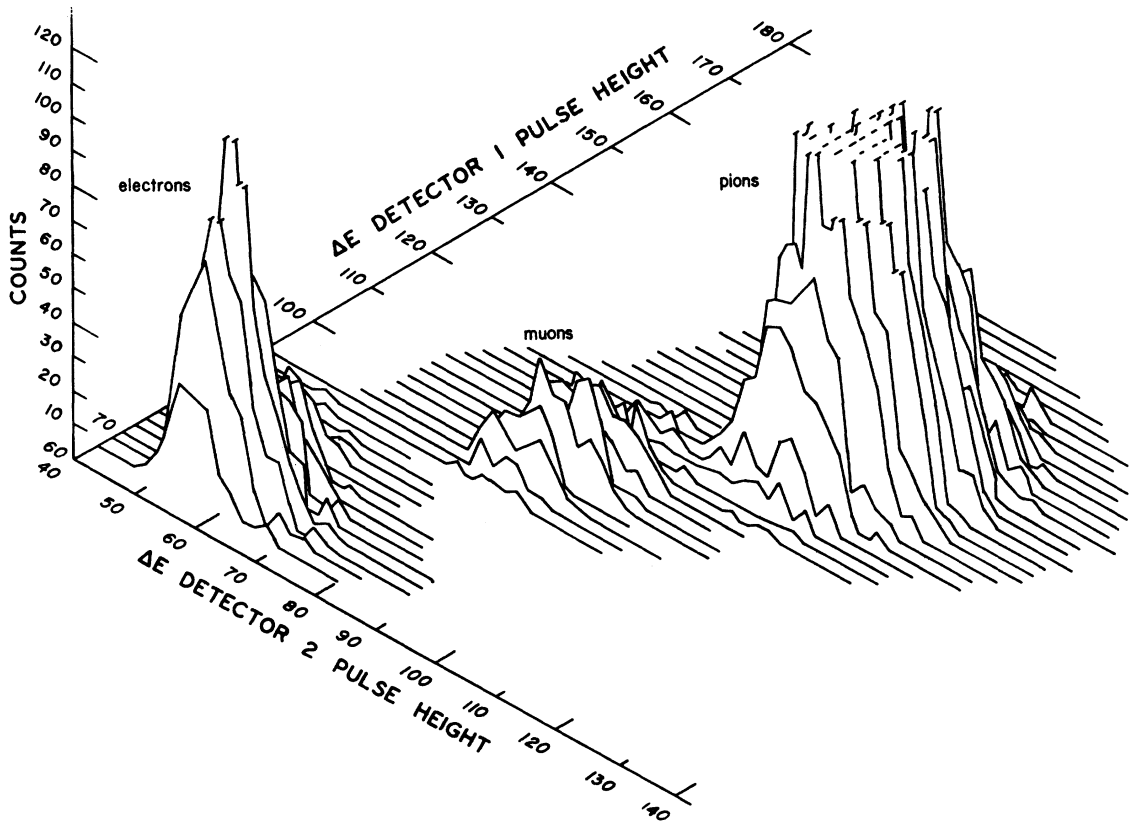

FIG. 1. Three-dimensional spectrum of in-beam telescope used for absolute calibration of relative monitors at 50 MeV.

surements showed the counters agreed to within statistics. A block diagram for this pion identification requirement is shown in Fig. 2. With one change in the orientation of the 10 detector telescopes, 18 angles were measured. Two telescopes were kept fixed in angle to check the relative normalization.

The analog signals from the ten telescopes were sent to CAMAC analog-to-digital converters and stored on magnetic tape event by event using a PDP-11/45 computer and the data acquisition program ZEUS.[24] The trigger system for the computer and the monitor events was disabled after a trigger and enabled by the computer after the processing of an event. Thus, it was necessary to correct only for the electronics dead time before the trigger system in calculating cross sections. This dead time was determined to be less than 1%.

All of the targets except ^{16}O were self-supporting foils. Natural carbon and CH_2 targets were used for the ^{12}C measurements, natural calcium was used for ^{40}Ca, and foils enriched to 97.6% in ^{90}Zr and 98.7% in ^{208}Pb were used for the heavier nuclei. The ^{16}O target was natural water in the form of a gel with 1.5% agar mixture. Background measurements were made using empty target frames.

III. DATA REDUCTION

The results for each detector telescope were reconstructed from the data tapes as a two-dimensional spectrum of ΔE versus E. A representative spectrum is shown in Fig. 3 for π^+ scattering from ^{16}O at 90°. The projection within the mask is shown in Fig. 4. The resolution of the detectors was nominally 1.2 MeV (FWHM). Backgrounds in the region of the ground state peak were usually negligible.

The differential cross section at each angle was calculated taking into account the finite angular acceptance of the telescopes, the efficiency of the detector system, the target angle, the amount of pion decay from the target to the detector, pion reactions in the detector, and the scattering of the pion out of the detector before it stopped. The results of the measurements are presented in Tables I and II. The laboratory energy (E_{LAB}) is the pion energy at the center of the target.

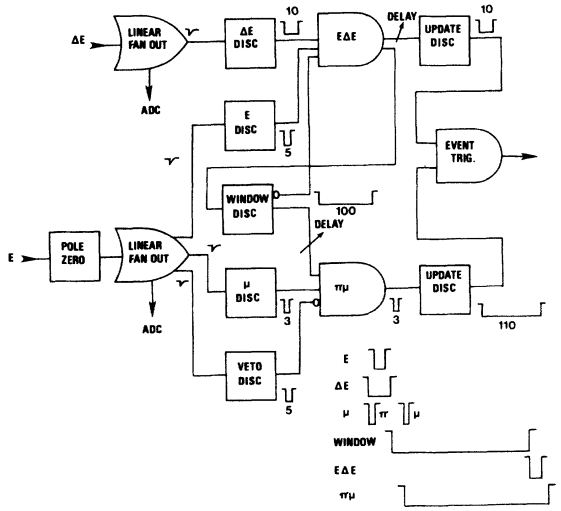

FIG. 2. Block diagram of electronics logic used for pion identification in the forward elastic scattering detectors.

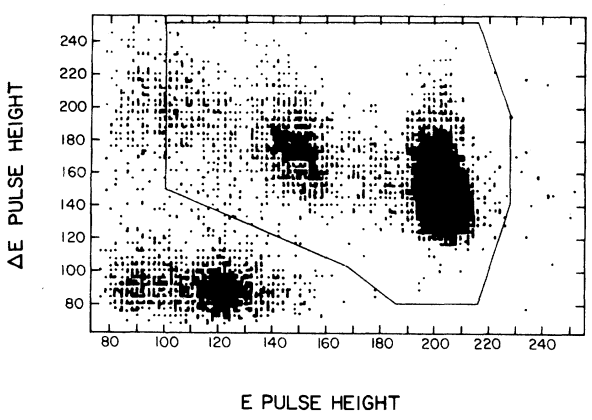

FIG. 3. Two-dimensional spectrum from a ΔE-E detector telescope showing the mask used to obtain the pion spectrum. The spectrum is that of ^{16}O measured at 90° for 50 MeV π^+.

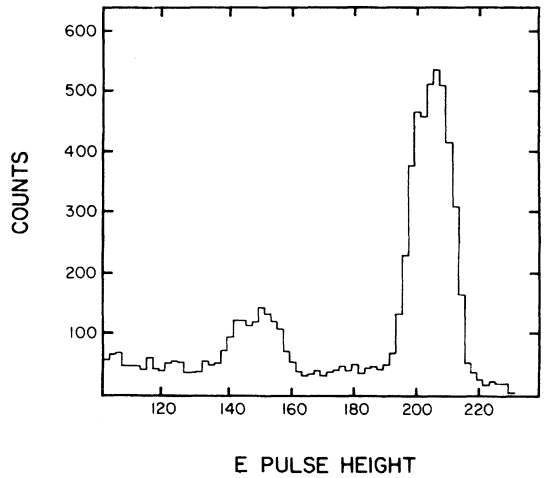

FIG. 4. E projection of the pion spectrum with the mask of Fig. 3.

TABLE I. Differential cross sections for π^+-nucleus elastic scattering—30 MeV. Scattering angles and cross sections are in the center of mass with units of degrees and mb/sr, respectively.

	^{12}C			^{16}O			^{40}Ca			^{90}Zr			^{208}Pb	
	E_{LAB} = 30.3 MeV			30.0 MeV			30.5 MeV			30.7 MeV			30.7 MeV	
$\theta_{c.m.}$	$\frac{d\sigma}{d\Omega}_{c.m.}$	$\Delta\sigma_{c.m.}$	$\theta_{c.m.}$	$\frac{d\sigma}{d\Omega}_{c.m.}$	$\Delta\sigma_{c.m.}$	$\theta_{c.m.}$	$\frac{d\sigma}{d\Omega}_{c.m.}$	$\Delta\sigma_{c.m.}$	$\theta_{c.m.}$	$\frac{d\sigma}{d\Omega}_{c.m.}$	$\Delta\sigma_{c.m.}$	$\theta_{c.m.}$	$\frac{d\sigma}{d\Omega}_{c.m.}$	$\Delta\sigma_{c.m.}$
25.4	23.3	2.7	30.3	16.2	1.6	25.1	235	18	25.1	954	71	25.0	4801	408
30.4	9.55	0.95	40.4	8.39	0.59	30.1	92.8	6.9	30.1	412	28	30.0	1851	143
40.6	3.25	0.35	45.4	6.22	0.37	40.2	44.4	2.8	40.1	173	11	40.0	664	46
45.6	3.01	0.23	55.5	5.40	0.16	45.2	33.2	2.1	45.1	110	7	45.0	383	25
55.7	2.73	0.14	60.5	4.60	0.13	55.2	26.8	0.8	55.1	67.3	1.9	55.0	180	5
60.8	2.65	0.13	70.6	5.69	0.14	60.2	23.1	0.7	60.1	53.9	1.5	60.0	118	4
70.8	3.50	0.14	80.6	6.14	0.15	70.2	21.8	0.6	70.1	37.2	1.2	70.1	62.6	1.9
80.9	4.02	0.15	85.6	6.91	0.17	80.3	19.8	0.6	80.1	26.9	0.9	80.1	33.8	1.4
85.9	4.52	0.16	90.6	6.98	0.17	85.3	20.3	0.6	85.1	22.6	0.8	85.1	26.0	1.5
90.9	4.60	0.17	100.6	8.46	0.21	90.3	17.5	0.5	100.1	16.8	0.5	90.1	22.1	1.2
100.9	6.07	0.19	105.6	8.47	0.21	100.3	19.0	0.6	105.1	15.2	0.4	100.1	18.7	1.0
105.8	6.50	0.21	110.6	9.05	0.23	105.3	16.5	0.5	110.1	13.3	0.7	105.1	17.3	1.2
110.8	6.68	0.21	120.5	9.82	0.25	110.2	15.9	0.5	120.1	13.5	0.7	110.1	18.5	1.1
120.8	7.42	0.23	130.5	10.2	0.25	120.2	14.5	0.5	130.1	14.1	0.7	120.0	18.9	1.3
130.7	8.48	0.26	140.4	10.4	0.26	130.2	13.7	0.5	140.1	16.7	0.9	130.0	20.6	1.3
140.6	9.32	0.28	150.3	9.93	0.47	140.2	13.0	0.5	150.1	19.4	1.4	140.0	23.3	1.6
150.4	8.87	0.44	160.2	10.5	0.56	150.1	13.1	0.8	160.0	14.8	2.0	150.0	26.0	2.2
160.3	9.93	0.55				160.1	8.8	0.9						

IV. ANALYSIS

A phenomenological optical model analysis was performed for all of the angular distributions presented here. The form of the πN t matrix used to calculate the optical potential was[4]

$$t(E(k),\vec{q},\vec{q}') \propto \sum_{i=0}^{1} b_i(E)(\vec{q}\cdot\vec{q}')^i \frac{(k^2+\alpha_i^2)^2}{(\alpha_i^2+q^2)(\alpha_i^2+q'^2)},$$

where α_i is a parameter indicating the πN interaction range ($\alpha_0=\alpha_1=\infty$ is the zero-range local limit of the Kisslinger potential), k and E are the

TABLE II. Differential cross sections for π^+-nucleus elastic scattering—50 MeV. Scattering angles and cross sections are in the center of mass with units of degrees and mb/sr, respectively.

			^{16}O			^{40}Ca			^{90}Ar			^{208}Pb		
E_{LAB}			49.7 MeV			50.0 MeV			49.9 MeV			49.9 MeV		
$\theta_{c.m.}$	$\frac{d\sigma}{d\Omega}_{c.m.}$	$\Delta\sigma_{c.m.}$	$\theta_{c.m.}$	$\frac{d\sigma}{d\Omega}_{c.m.}$	$\Delta\sigma_{c.m.}$	$\theta_{c.m.}$	$\frac{d\sigma}{d\Omega}_{c.m.}$	$\Delta\sigma_{c.m.}$	$\theta_{c.m.}$	$\frac{d\sigma}{d\Omega}_{c.m.}$	$\Delta\sigma_{c.m.}$	$\theta_{c.m.}$	$\frac{d\sigma}{d\Omega}_{c.m.}$	$\Delta\sigma_{c.m.}$
30.5	8.98	0.43	25.3	15.80	0.88	25.1	77.25	3.63	25.1	342	22	25.0	1231	87
35.6	8.69	0.43	30.4	13.43	0.60	30.1	46.72	2.03	30.1	202	11	30.0	651	35
40.6	7.13	0.33	40.5	10.20	0.44	40.2	31.06	1.37	40.1	83.5	4.3	40.0	200	10
45.7	5.80	0.30	45.5	7.76	0.33	45.2	22.68	1.00	45.w	57.2	2.7	45.0	86	4.5
55.8	3.43	0.17	55.6	4.36	0.08	55.2	12.65	0.44	55.1	24.1	0.8	55.1	18.6	1.0
60.8	2.80	0.14	60.6	3.97	0.07	60.3	10.63	0.31	60.1	19.0	0.6	60.1	6.61	0.53
70.9	2.63	0.12	70.7	4.19	0.07	70.3	10.31	0.30	70.1	11.7	0.5	70.1	2.74	0.44
81.0	3.86	0.07	80.7	5.88	0.09	80.3	9.97	0.32	80.1	7.40	0.38	80.1	3.27	0.43
86.0	4.66	0.11	85.7	6.51	0.09	85.3	9.48	0.33	85.1	5.36	0.38	85.1	6.09	0.55
91.0	5.11	0.05	90.7	7.17	0.16	90.3	8.27	0.18	90.1	4.29	0.35	90.1	9.61	0.59
101.0	6.37	0.11	100.7	8.02	0.17	100.3	6.26	0.17	100.1	6.32	0.42	100.1	13.8	0.7
105.9	6.45	0.13	105.7	7.84	0.17	105.3	4.42	0.20	105.1	7.37	0.38	105.1	12.9	0.7
110.9	6.64	0.13	110.7	7.67	0.12	110.3	3.72	0.20	110.1	8.88	0.46	110.1	13.7	0.7
120.8	6.59	0.13	120.6	6.65	0.08	120.3	2.59	0.21	120.1	12.8	0.5	120.1	11.7	0.7
130.7	6.07	0.12	130.6	5.62	0.09	130.2	3.10	0.25	130.1	14.0	0.6	130.0	12.3	0.8
140.6	5.47	0.25	140.5	4.71	0.09	140.2	3.79	0.29	140.1	14.2	0.6	140.0	12.4	0.6
150.5	4.94	0.11	150.5	3.83	0.07	150.2	4.91	0.26	160.1	11.8	0.8	150.0	15.9	1.6
160.3	4.39	0.08	160.3	3.29	0.07	160.1	6.12	0.31				160.0	18.0	1.5

on-shell pion momentum and energy, $\vec{q}$ and $\vec{q}'$ are the off-shell initial and final pion momenta, and b_0 and b_1 are the complex s- and p-wave strengths which are treated as free parameters. Acceptable fits were found with values of α_i from 300 MeV/c to 700 MeV/c, but the fit is rather insensitive to the exact value in this range. In the calculations presented here, $\alpha_0 = \alpha_1 = 500$ MeV/c. The search code[4] varies the strength parameters b_0 and b_1 to minimize χ^2 between the calculated and the experimental angular distributions. For these fits, the nuclear density was taken to be a Woods-Saxon form

$$\rho(r) \propto (1 + e^{(r-c)/a})^{-1},$$

where c is the half-density radius and a is the diffusivity. For the calculations presented here, the parameters used were: (a) ^{12}C, $c = 2.5$ fm, $a = 0.37$ fm; (b) ^{16}O, $c = 2.7$ fm, $a = 0.41$ fm; (c) ^{40}Ca, $c = 3.68$ fm, $a = 0.58$ fm; (d) ^{90}Zr, $c = 4.86$ fm, $a = 0.57$ fm; and (e) ^{208}Pb, $c = 6.40$ fm, $a = 0.54$ fm. For ^{12}C and ^{16}O, the Gaussian charge distribution of the proton was subtracted from the Woods-Saxon charge distribution determined from electron scattering. This subtraction was done via the method of Gibbs *et al.*,[4] to obtain the values of c and a given above. The distributions for ^{40}Ca, ^{90}Zr, and ^{208}Pb were taken from Ref. 3. The parabolic parameter was not used since the calculations showed very little sensitivity to small changes in the density.

In Figs. 5 and 6 we present the calculations of the phenomenological optical potentials with the experimental angular distributions. In general,

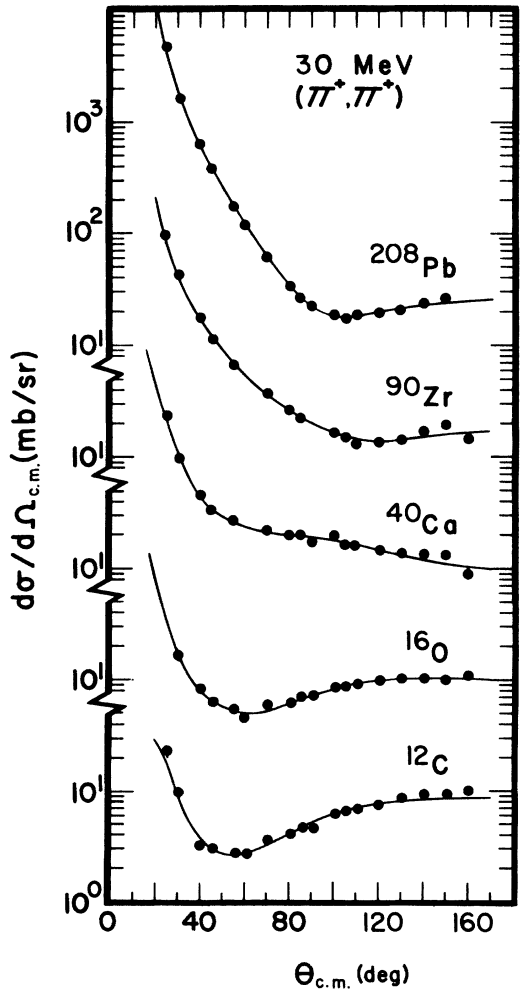

FIG. 5. Angular distributions for elastic scattering at 30 MeV. The curves are from a phenomenological optical model calculation.

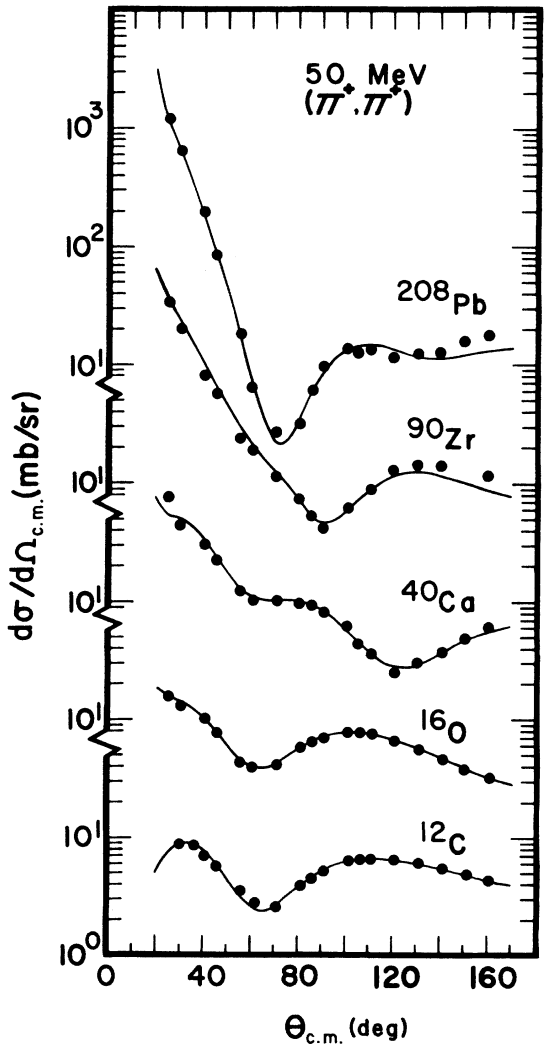

FIG. 6. Angular distributions for elastic scattering at 50 MeV. The curves are from a phenomenological optical model calculation.

TABLE III. Phenomenological optical model parameters for 30 and 50 MeV π^+-elastic scattering. Uncertainties were determined from fits having comparable values of χ^2 but different starting parameters. They are less than 5% for $\mathrm{Re}b_0$ and $\mathrm{Re}b_1$, less than 20% for $\mathrm{Im}b_1$, and approximately 50% for $\mathrm{Im}b_0$. These uncertainties are much larger than those obtained from simple statistical criteria.

Nucleus	Energy (MeV)	$\mathrm{Re}b_0$ (fm^3)	$\mathrm{Im}b_0$ (fm^3)	$\mathrm{Re}b_1$ (fm^3)	$\mathrm{Im}b_1$ (fm^3)	χ^2/n_D
^{12}C	30	−4.13	−0.04	6.26	1.22	2.8
	50	−3.26	0.46	6.60	0.69	1.3
^{16}O	30	−4.14	−0.13	6.51	1.55	2.8
	50	−3.42	−0.04	6.78	1.26	1.1
^{40}Ca	30	−4.01	0.08	6.00	0.58	3.1
	50	−3.51	0.16	7.05	0.62	4.4
^{90}Zr	30	−3.24	0.54	5.85	0.88	1.6
	50	−3.05	0.49	6.96	1.82	10.5
^{208}Pb	30	−1.16	0.03	4.96	1.96	1.2
	50	−1.91	0.04	5.54	1.11	3.0

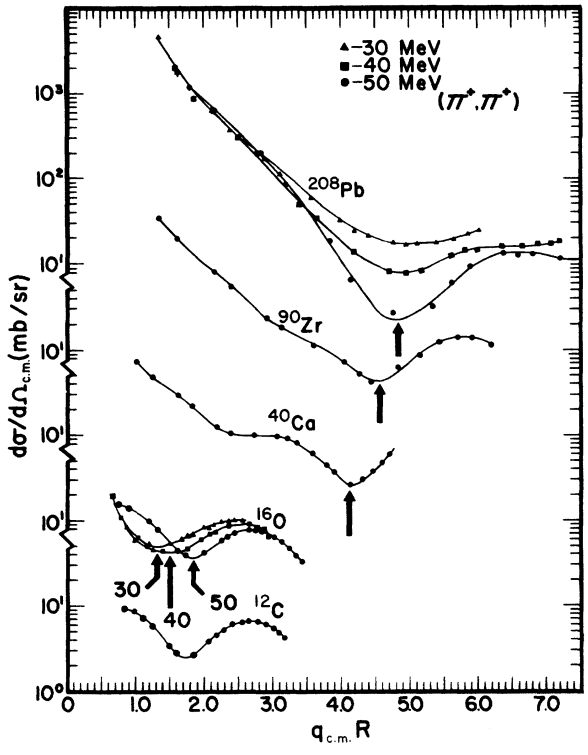

FIG. 7. Angular distributions as a function of $q_{c.m.}R$, where $q_{c.m.}$ is the momentum transfer in the center of mass. The curves are the results of phase-shift fits. The arrows indicate the minima in the distributions.

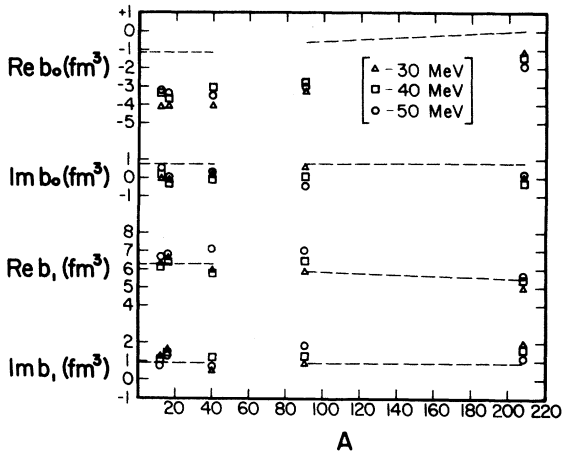

FIG. 8. Strength parameters of the phenomenological optical model discussed in the text.

the agreement with the data is quite satisfactory. The complex strengths b_0 and b_1 are presented in Table III. It should be noted that although some of the values of $\mathrm{Im}b_0$ are negative and thus pion producing, all of the potentials are unitary.

One striking feature between Fig. 5 at 30 MeV and Fig. 6 at 50 MeV is the increased structure of the angular distributions at 50 MeV. The minimum near 60° is the result of the interference between the repulsive s-wave strength and the attractive p-wave strength. This minimum is not clearly seen for ^{90}Zr and ^{208}Pb because of the appearance of the first diffraction minimum. The diffraction character can be displayed by plotting the angular distribution as a function of momentum transfer (qR) as is done in Fig. 7. The curves are phase-shift fits calculated as described in Ref. 25. For the ^{208}Pb distribution, the large-angle minimum is essentially constant with qR as expected for a diffraction minimum, whereas the "s-p wave" interference minimum is constant in angle and not in momentum transfer as is seen for ^{16}O.

The values of the fitted complex strengths b_0 and b_1 are displayed in Fig. 8 as a function of A. For comparison, the values obtained at 40 MeV (Ref. 13) are also included in the figure. The dashed lines are values of the parameters b_0 and b_1 calculated at 40 MeV using free πN scattering data in an impulse approximation.[26] The phenomenological parameters agree qualitatively with the free πN strengths except for $\mathrm{Re}b_0$ which the data want to be much more repulsive. Also, as was previously pointed out,[13] the isospin dependence $(N-Z)/A$ of the phenomenological parameters is essentially that predicted by the free πN strengths in the impulse approximation.

ACKNOWLEDGMENTS

The authors would like to thank the staff of LAMPF for their support during the preparation and execution of these experiments. We acknowledge many discussions with G. Stephenson and W. R. Gibbs concerning the use of the non-local optical model code. This work was supported by the National Science Foundation (South Carolina, and Virginia Polytechnic Institute and State University), by the Department of Energy (LASL), and by the Union Carbide Corporation under Contract No. W-7405-eng-26 with the Department of Energy (ORNL).

---

*Present address: Los Alamos Scientific Laboratory, Los Alamos, New Mexico 87545.
†Present address: Nichols State University, Thibodaux, Louisiana 70301.
‡On leave from Tel Aviv University, Ramat Aviv, Israel.
§Present address: Physics Department and Laboratory for Nuclear Science, Massachusetts Institute of Technology, Cambridge, Massachusetts 02139.
¶Present address: Spire Corporation, Bedford, Massachusetts 01730.

[1]K. Stricker, H. McManus, and J. A. Carr, Phys. Rev. C 19, 929 (1979).
[2]G. E. Brown, B. K. Jennings, and V. Rostokin, LAMPF Summer School on Nuclear Structure with Pions and Protons, June 1977, edited by R. L. Burman and B. F. Gibson, V. LASL Report LA-6926-C (unpublished).
[3]N. J. Digiacomo, A. S. Rosenthal, E. Rost, and D. A. Sparrow, Phys. Lett. 66B, 421 (1977).
[4]W. R. Gibbs, B. F. Gibson, and G. J. Stephenson, Jr., Phys. Rev. Lett. 39, 1316 (1977).
[5]Tsung-Shung H. Lee and Soumya Chakravarti, Phys. Rev. C 16, 273 (1977).
[6]L. C. Liu and C. M. Shakin, Phys. Rev. C 16, 333 (1977).
[7]Gerald A. Miller, Phys. Rev. C 16, 2325 (1977); 18, 579 (1978).
[8]L. C. Liu, Phys. Rev. C 17, 1787 (1978).
[9]R. H. Landau and A. W. Thomas, Phys. Lett. 61B, 364 (1976); A. W. Thomas and R. H. Landau, Phys. Rep. 58, 122 (1980).
[10]L. C. Liu and C. M. Shakin, Phys. Rev. C 19, 129 (1979).
[11]D. J. Malbrough, C. W. Darden III, R. D. Edge, T. Marks, B. M. Preedom, F. E. Bertrand, T. P. Cleary, E. E. Gross, C. A. Ludemann, K. Gotow, R. L. Burman, M. A. Moinester, and R. P. Redwine, Phys. Rev. C 17, 1395 (1978).
[12]M. A. Moinester, R. L. Burman, R. P. Redwine, M. A. Yates-Willimas, D. J. Malbrough, C. W. Darden III, R. E. Edge, T. Marks, S. H. Dam. B. M. Preedom, F. E. Bertrand, T. P. Cleary, E. E. Gross, C. A. Ludemann, M. Blecher, K. Gotow, D. Jenkins, and F. Milder, Phys. Rev. C 18, 2678 (1978).
[13]M. Blecher, K. Gotow, D. Jenkins, F. Milder, F. E. Bertrand, T. P. Cleary, E. E. Gross, C. A. Ludemann, M. A. Monester, R. L. Burman, M. Hamm, R. P. Redwine, M. Yates-Williams, S. Dam, C. W. Darden III, R. D. Edge, D. J. Malbrough, T. Marks, and B. M. Preedom, Phys. Rev. C 20, 1884 (1979).
[14]S. A. Dytman, J. F. Amann, P. D. Barnes, J. N. Craig, K. G. R. Doss, R. A. Eisenstein, J. D. Sherman, W. R. Wharton, G. R. Burleson, S. L. Verbeck, R. J. Peterson, and H. A. Thiessen, Phys. Rev. C 18, 2316 (1978); S. A. Dytman, J. F. Amann, P. D. Barnes, J. N. Craig, K. G. R. Doss, R. A. Eisenstein, J. D. Sherman, W. R. Wharton, G. R. Burleson, S. L. Verbeck, R. J. Peterson, and H. A. Thiessen, *ibid.* 19, 971 (1979).
[15]R. R. Johnson, T. G. Masterson, K. L. Erdman, A. W. Thomas, and R. H. Landau, Nucl. Phys. A296, 444 (1978); R. R. Johnson, T. Masterson, B. Bassalleck, W. Gyles, T. Marks, K. L. Erdman, A. W. Thomas, D. R. Gill, E. Rost, J. J. Kraushaar, J. Alster, C. Saber, J. Arvieux, and M. Krell, Phys. Rev. Lett. 43, 844 (1979).
[16]B. M. Preedom, *Proceedings of the Seventh International Conference on High Energy Physics and Nuclear Structure*, edited by M. P. Locher (Birkhauser, Basel, Switzerland, 1977), p. 119.
[17]R. P. Redwine, *Meson-Nuclear Physics*—1979 (Houston), Proceedings of the 2nd International Topical Conference on Meson-Nuclear, edited by E. V. Hungerford III (AIP, New York, 1979), p. 501.
[18]F. E. Bertrand *et al.* (unpublished).
[19]R. L. Burman, R. L. Fulton, and M. Jakobson, Nucl. Instrum. Methods 131, 29 (1975).
[20]G. J. Krausse and P. A. M. Gram, Nucl. Instrum. Methods 156, 265 (1978).
[21]E. A. Wadlinger, Nucl. Instrum. Methods 134, 243 (1976).
[22]M. J. Saltmarsh, B. M. Preedom, R. D. Edge, and C. W. Darden III, Nucl. Instrum. Methods 105, 311 (1972).
[23]D. Axen, G. Duesdieker, L. Felawka, C. H. Q. Ingram, G. Jones, M. Salomon, and W. Westlund, Nucl. Instrum. Methods 118, 435 (1974).
[24]B. M. Preedom, ZEUS, a data acquisition code for a PDP-11/45 (unpublished).
[25]W. R. Gibbs, B. F. Gibson, and G. J. Stephenson, Jr., Phys. Rev. C 18, 2782 (1978).
[26]E. H. Auerbach, D. M. Fleming, and M. M. Sternheim, Phys. Rev. 162, 1683 (1967); G. Rowe, M. Salomon, and R. H. Landau, Phys. Rev. C 18, 584 (1978).